Structure, Function, and Aggregation of the Zinc-Free Form of the p53 DNA Binding Domain†

James S. Butler and Stewart N. Loh*

Department of Biochemistry and Molecular Biology, State University of New York Upstate Medical University, 750 East Adams Street, Syracuse, New York 13210

Received August 14, 2002; Revised Manuscript Received December 4, 2002

ABSTRACT: The p53 DNA binding domain (DBD) contains a single bound zinc ion that is essential for activity. Zinc remains bound to wild-type DBD at temperatures below 30 °C; however, it rapidly dissociates at physiological temperature. The resulting zinc-free protein (apoDBD) is folded and stable. NMR spectra reveal that the DNA binding surface is altered in the absence of Zn^{2+}. Fluorescence anisotropy studies show that Zn^{2+} removal abolishes site-specific DNA binding activity, although full nonspecific DNA binding affinity is retained. Surprisingly, the majority of tumorigenic mutations that destabilize DBD do not appreciably destabilize apoDBD. The R175H mutation instead substantially accelerates the rate of Zn^{2+} loss. A considerable fraction of cellular p53 may therefore exist in the folded zinc-free form, especially when tumorigenic mutations are present. ApoDBD appears to promote aggregation of zinc-bound DBD via a nucleation-growth process. These data provide an explanation for the dominant negative phenotype exhibited by many mutations. Through a combination of induced p53 aggregation and diminished site-specific DNA binding activity, Zn^{2+} loss may represent a significant inactivation pathway for p53 in the cell.

The transcription factor p53 (393 amino acids) regulates expression of a host of genes involved in cell cycle control and apoptosis. Its function is to maintain the integrity of the genome. It does so by preventing cells with damaged DNA from replicating, either by pausing the cell cycle to allow for necessary repairs or by promoting apoptosis if repairs cannot be made (*1*−*6*). This activity ensures that excessive mutations do not accumulate in daughter cells to the point where they may become cancerous.

p53 is mutated in over one-half of all tumors. The overwhelming majority of these changes are found in the central DNA binding domain (DBD)[1] comprised of residues 94−312 (*7*). While it is clear that tumorigenic DBD mutations act by diminishing p53's site-specific DNA binding activity (*8*, *9*), the mechanisms by which they do so are not fully characterized. Some mutations (e.g., R273H) decrease binding affinity simply by eliminating critical protein−DNA contacts (*7*, *10*, *11*). Others (e.g., R175H) lower thermodynamic stability to the point where DBD is predicted to be substantially unfolded at physiological temperature (*12*). A third mechanism is suggested by previous studies which report that some mutations appear to enhance loss of the single bound zinc ion (*13*). The purpose of this paper is to test the hypothesis that Zn^{2+} loss may represent a significant pathway of p53 inactivation.

The DBD X-ray crystal structure reveals that Zn^{2+} is coordinated to C176 and H179 of the L2 loop and to C238 and C242 of the L3 loop (Figure 1) (*7*). The L3 loop binds the DNA minor groove. The L2 loop does not interact with DNA but makes extensive contacts with the L3 loop and the β-sheet scaffold. Zinc therefore appears to hold the L3 loop in the proper orientation for minor groove binding. A number of studies support the idea that Zn^{2+} is necessary for transcriptional activation. The presence of metal chelating agents, the Zn^{2+}-binding protein metallothionein, or Zn^{2+} binding site mutations reduce DNA binding affinity in vitro (*14*−*17*) and in vivo (*16*−*18*). Moreover, some tumorigenic DBD mutations enhance inactivation by chelating compounds (*15*), suggesting that they may increase the rate of Zn^{2+} release or decrease its overall binding affinity.

In this study, we characterize the structure, stability, and function of zinc-free DBD (apoDBD) in order to provide a comprehensive framework for interpreting the effects of mutation on p53 activity. We have chosen to analyze five of the six most prevalent tumorigenic mutations present in the general population (*7*). These positions (R175, G245, R248, R249, R282; Figure 1) account for 22% of the 15000 p53 mutations identified from human tumors and cell lines according to the database compiled by the Institut Curie (http://p53.curie.fr/). The fact that four of the five sites (all except R282) are located in the Zn^{2+}-binding L2 and L3 loops emphasizes the need to understand the role that Zn^{2+} loss plays in p53-mediated cancers.

MATERIALS AND METHODS

Gene Construction and Mutagenesis. The human p53 DBD gene construct was cloned from plasmid pHP53B (American Type Culture Collection) with primers 5′-CCCCTCTGGC-

† This work was funded by U.S. Department of Defense Grant DAMD17-98-1-8558.

* To whom correspondence should be addressed. E-mail: lohs@upstate.edu. Tel: (315) 464-8731. Fax: (315) 464-8736.

[1] Abbreviations: DBD, DNA binding domain of p53 (residues 94−312) containing a single bound Zn^{2+}; apoDBD, DBD with Zn^{2+} removed; PAR, 4-(2-pyridylazo)resorcinol; CD, circular dichroism; NMR, nuclear magnetic resonance; HSQC, heteronuclear single-quantum correlation.

10.1021/bi026635n CCC: $25.00
Published on Web 02/01/2003

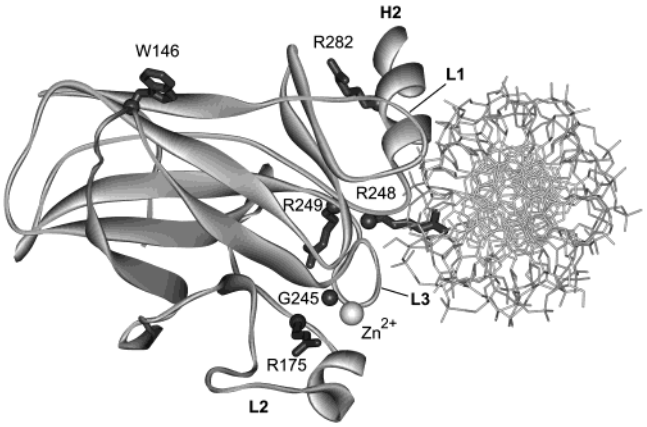

FIGURE 1: X-ray crystal structure of the wt DBD/DNA complex (*7*) showing locations of mutations (dark gray). Helices and loops near the Zn^{2+} and DNA binding sites are labeled; Zn^{2+} is represented as a light gray sphere. W146 is also shown.

TATGTCATCTTCTGTCCCT-3′ and 5′-GCTGGGGAGA-GTCGACTTAGGTGTTGTTGGGCAG-3′ (Integrated DNA Technologies). The cloned gene was cleaved with *Nde*I and *Sal*I (New England Biolabs) and inserted into plasmid pET23a (Novagen). Mutant p53 genes were constructed using the QuikChange site-directed mutagenesis kit (Stratagene) and fully sequenced.

Protein Expression and Purification. Proteins were expressed in the *Escherichia coli* strain BL21(DE3) (Novagen). Cultures were grown at 30 °C in Luria−Bertani media (*19*) until $Abs_{600} = 1.0$, at which point the temperature was lowered to 18 °C and 100 mg/L isopropyl β-D-thiogalactoside was added to induce protein expression. Cells were harvested by centrifugation 18 h later and purified as previously described (*10*). Protein samples were judged to be >95% pure by sodium dodecyl sulfate−polyacrylamide gel electrophoresis with staining by Coomassie brilliant blue (not shown). Protein concentration was determined by absorbance at 280 nm using a calculated extinction coefficient of 15930 M^{-1} cm^{-1} in 6 M guanidine hydrochloride (*20*). NMR samples were prepared identically except cultures were grown in M9 media (*19*) containing 1 g/L $(^{15}NH_4)_2SO_4$ (Cambridge Isotope Laboratories).

ApoDBD was prepared by treating DBD with $^1/_{33}$ volume of 10% acetic acid (final pH 4.3) and $^1/_{100}$ volume of 0.5 M EDTA and incubating for 1 min on ice. The pH was then raised to 6.7 by addition of 1.5 volumes 0.5 M bis-tris propane (Sigma) (pH 6.8). The resulting zinc-free protein was then desalted into the indicated buffers using a PD-10 column (Pharmacia). Residual levels of Zn^{2+} were undetectable by assays employing the chromogenic Zn^{2+}-binding reagent 4-(2-pyridylazo)resorcinol (PAR), as described below.

Zinc Dissociation Assays. Data were collected on a Varian Cary-100 spectrophotometer equipped with a thermoelectrically heated sample holder. Zinc release kinetics were performed in 50 mM bis-tris propane (pH 6.8), 0.5 M NaCl, 5 mM dithiothreitol, and 0.5 mM PAR at the temperatures indicated in Figure 2. The fraction of Zn^{2+} released was calculated by normalizing the absorbance readings to that of an identical sample containing 625 μM methyl methanethiosulfonate (Sigma), which alkylates cysteine residues and fully liberates bound Zn^{2+}. All mutants except for R175H were found by this assay to contain 1.0 ± 0.05 equiv of bound Zn^{2+} immediately after purification (not shown), using $\Delta\epsilon_{500} = 6.6 \times 10^4$ M^{-1} cm^{-1} (*21*). R175H contained only 0.85 ± 0.05 mol of Zn^{2+}/mol of protein.

DNA Binding Assays. DNA binding affinities were determined by monitoring the change in fluorescence anisotropy of 5′-fluorescein-labeled oligomers containing consensus *gadd*45 (5′-AATATGGGAACATGTCTAAGCATGCTGT-TG-3′) (*22*) and nonconsensus (5′-AATATGGTTTGAAT-AAAGAGTAAAGATTTG-3′) (*23*) binding sequences (Integrated DNA Technologies). DNA concentration was fixed at 50 nM, and DBD concentration was varied from 0 to 30 μM. Solution conditions were 50 mM *N*-(2-hydroxyethyl)-piperazine-*N*′-2-ethanesulfonic acid (pH 6.8), 0.1 M NaCl, and 5 mM dithiothreitol (DTT). Data were collected at 10 °C on a Jobin-Yvon/SPEX Fluoromax-3 fluorometer with excitation and emission wavelengths of 490 and 525 nm, respectively, and slit widths set to 5 nm band-pass. Dissociation constants were calculated by fitting the data to a simple one-site binding equation using the Origin program (Microcal).

Equilibrium Folding Experiments. To minimize protein concentration errors, samples were prepared by adding equal volumes of DBD to either 50 mM bis-tris propane (pH 6.8), 0.1 M NaCl, and 5 mM DTT or to the same buffer containing 5 M urea (Sigma, ultrapure grade). The solutions were then mixed in various ratios using a Hamilton Microlab 540B dispenser to yield the final indicated urea concentrations. Final protein concentrations were 1−2 μM. Urea concentrations were determined by refractive index measurements (*24*). Samples were incubated for at least 12 h at 10 °C prior to data collection. Tryptophan fluorescence spectra were generated by exciting at 280 nm and recording emission from 300 to 425 nm (10 °C). Both slits were set to 4 nm band-pass. Emission spectra were integrated from 325 to 375 nm and plotted against urea concentration. Thermodynamic parameters were obtained by fitting these data to the linear extrapolation equation using the Origin software (*25*).

Aggregation Experiments. Sample conditions were 50 mM bis-tris propane (pH 6.8), 0.1 M NaCl, and 5 mM dithiothreitol, 37 °C, with protein and urea concentrations indicated in the figure legends. To avoid protein aggregation prior to the start of the experiment, samples were kept on ice and added to a prewarmed cuvette, whereupon a 10-fold excess of prewarmed buffer was immediately added and data collection begun.

RESULTS AND DISCUSSION

Mutation and Elevated Temperature Enhance the Rate of Zinc Release. Fersht and colleagues have shown that, at 10 °C and micromolar DBD concentration, Zn^{2+} does not appreciably dissociate from wild-type (wt) and mutant proteins even when they are unfolded in 6 M urea (*10*). To more closely approximate cellular conditions, we monitored Zn^{2+} loss at higher temperatures and in the presence of the chelating agent PAR. Two PAR molecules bind one Zn^{2+} with $K_{d,1} = 0.25$ μM and $K_{d,2} = 1.8$ μM, and the resulting complex absorbs at 500 nm. The rapid second-order rate constant of 2×10^7 M^{-1} s^{-1} for formation of the 1:1 species ensures that the observed reaction rate is not limited by PAR/Zn^{2+} binding. Figure 2 shows that the rate of Zn^{2+} loss from

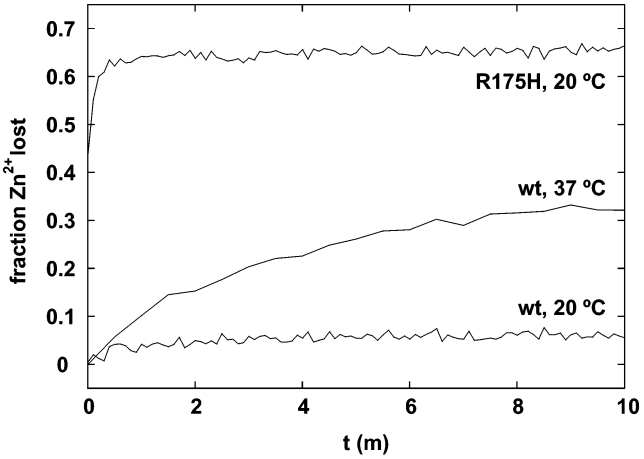

FIGURE 2: Kinetics of Zn^{2+} release from wt and R175H DBD determined by PAR assays. DBD and PAR concentrations are 2 μM and 0.5 mM, respectively.

wt DBD increases dramatically with temperature. At 20 °C, this rate is too slow to be measured in the presence of 0.5 mM PAR. In contrast, ~30% of Zn^{2+} is lost within 5 min of heating at 37 °C; the remainder appears to dissociate on a slower time scale. There are at least two potential causes of the biphasic kinetics. One is that there are two populations of DBD with different Zn^{2+} dissociation rates. Alternately, the fractional amplitude may reflect equilibrium partitioning of Zn^{2+} between DBD and PAR. We tested these models by repeating the experiment with 0.1 and 0.2 mM PAR. The observed amplitudes decreased with decreasing PAR concentration (not shown), consistent with the equilibrium partitioning model. Zinc dissociation constants, however, could not be determined quantitatively by this method. ApoDBD readily aggregates at 37 °C, and the resulting light scatter began to interfere with the absorbance measurements beyond the 10 min time scale indicated in Figure 2. We also attempted to measure K_d values by titrating apoDBD with $ZnCl_2$ and monitoring ligand−metal charge-transfer absorbance bands at 200−230 nm. These experiments failed because addition of more than 2−3 equiv of $ZnCl_2$ led to sample turbidity. This phenomenon has been observed with other Zn^{2+}-binding proteins and was attributed to intermolecular metal ion binding to surface cysteine and histidine residues (*26*, *27*). As a result, wt and mutant Zn^{2+} dissociation constants could not be directly compared.

Nevertheless, it is clear that the R175H mutant loses Zn^{2+} more rapidly than does wt at all temperatures (Figure 2). Both the rate constant and amplitude of the initial phase are greater for R175H at 20 °C than they are for wt at 37 °C. In total, these data suggest that cellular p53 may lose Zn^{2+} to other intracellular metal binding proteins on a functionally relevant time scale. This phenomenon will be much more pronounced in the case of R175H.

Structure and Function of ApoDBD. Figure 2 raises the possibility that a significant fraction of p53 may exist in the zinc-free state under physiological conditions. It is therefore appropriate to characterize the structure and properties of this form. To this end, we removed Zn^{2+} by lowering pH to 4.3 in the presence of 5 mM EDTA (4 °C). Circular dichroism (CD) spectra reveal that DBD adopts an alternate folded conformation below pH 5.5 (data not shown) which binds Zn^{2+} weakly, thus facilitating its rapid abstraction by

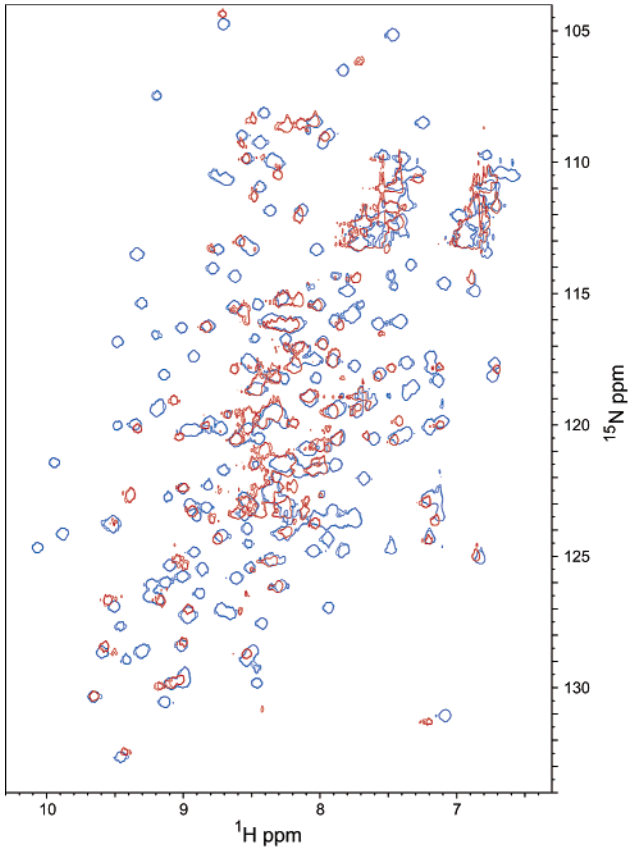

FIGURE 3: 600 MHz $^{15}N/^{1}H$ HSQC NMR spectra of zinc-bound (blue) and zinc-free (red) wt DBD. Sample conditions are 150 μM DBD, 80 μM apoDBD, 50 mM bis-tris propane (pH 6.8), 0.1 M NaCl, 10 mM dithiothreitol, and 5% $^{2}H_2O$ at 15 °C.

EDTA. Native apoDBD is then regenerated by raising pH to 6.8 and passing the solution through a gel filtration column to remove Zn^{2+} and EDTA. Full removal of Zn^{2+} was confirmed by subsequent PAR assays. DBD refolds reversibly when pH is lowered and raised in the absence of EDTA (not shown). Any changes in structure are therefore due to Zn^{2+} removal and not simply to exposure to acidic solution.

To determine the effects of Zn^{2+} removal on DBD structure, we recorded $^{15}N/^{1}H$ heteronuclear single-quantum correlation (HSQC) NMR spectra of the zinc-bound and zinc-free proteins (Figure 3). Since chemical shifts are extremely sensitive to structural changes, cross-peaks that shift by less than 0.1 ppm (^{1}H) and 0.5 ppm (^{15}N) likely represent regions of backbone structure that are similar in the two proteins. These residues are colored blue on the X-ray crystal structure of DBD in Figure 4. Red areas indicate amino acids whose resonances appear to shift by more than those limits. It must be pointed out that we could not obtain resonance assignments for apoDBD due to its limited solubility. Nevertheless, the pattern of chemical shift changes allows us to draw several conclusions with reasonable confidence. Residues near the Zn^{2+} binding site (including those in the L2 and L3 loops) exhibit widespread shifts. In contrast, many amino acids within the β-sheet scaffold do not shift, particularly those farther away from the Zn^{2+} binding site. This trend is consistent with the observation that the fluorescence emission spectra of W146, located on the opposite side of the β-sandwich from the metal binding region (Figure 1), are nearly identical for both DBD and apoDBD (not shown). Also unaffected are helix H2 and loop L1, which bind in

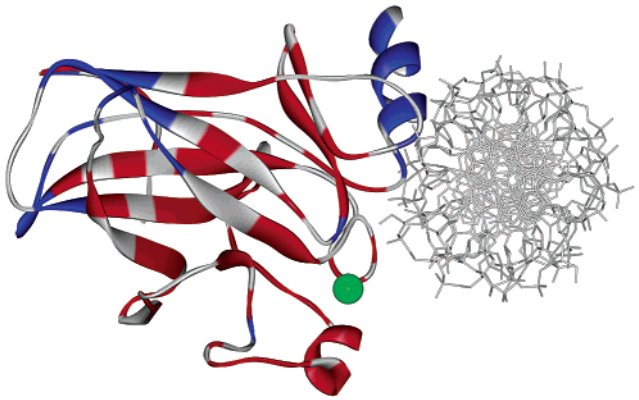

FIGURE 4: Effect of Zn^{2+} removal on DBD structure. DBD is shown in the same orientation as in Figure 1. Red regions represent residues whose $^{15}N/^{1}H$ HSQC cross-peaks shifted by more than 0.1 ppm (^{1}H) and 0.5 ppm (^{15}N). Blue indicates regions of structural similarity where resonances shifted by less than those amounts. The zinc ion is colored green. No information is available for the gray areas due to peak overlap or missing assignments.

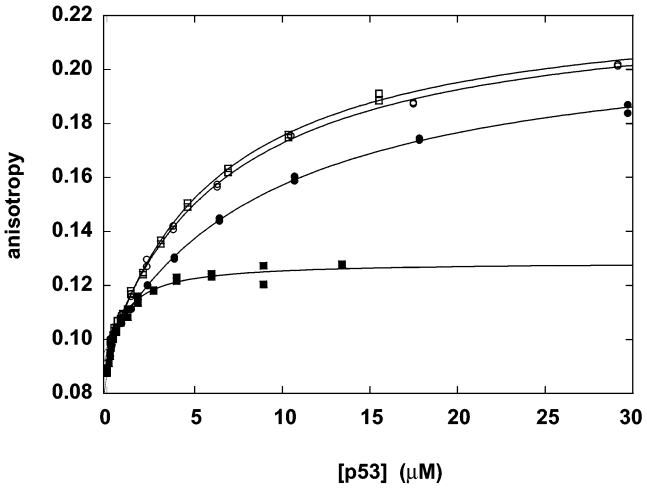

FIGURE 5: DNA binding of wt DBD (closed symbols) and wt apoDBD (open symbols) to 5′-fluorescein-labeled *gadd*45 (squares) and nonconsensus (circles) oligonucleotides. Lines are best fits of the data to a one-site binding model.

the DNA major groove. The secondary structure elements comprising the DNA binding surface thus appear to be independently structured. Removal of the metal ion disrupts the minor groove binding loop but not the major groove binding motif.

To test the functional consequence of Zn^{2+} loss, we measured DNA dissociation constants using 5′-fluorescein-labeled 30-mer oligonucleotides bearing nonconsensus and *gadd*45 binding sequences. DBD·DNA complex formation is monitored by the increase in fluorescence anisotropy of the fluorescein group (Figure 5). In all cases data are well-fit by a simple one-site binding equation, as indicated by the solid lines. The anisotropy of the complex, however, is higher for the nonconsensus oligonucleotide than it is for the *gadd*45 sequence. This result suggests that more than one protein molecule may bind to the former. A 30-mer oligonucleotide can in principle accommodate multiple nonspecific binding sites, since DBD interacts with ~9 base pairs according to the crystal structure (*7*). In contrast, tight binding of one DBD molecule to the *gadd*45 sequence in the center of the oligonuclotide may sterically prevent other molecules from binding nonspecifically to the flanking sequences.

Surprisingly, DBD and apoDBD possess similar apparent K_d values for the nonconsensus oligonucleotide (9.6 ± 1 μM and 6.8 ± 1 μM, respectively). DBD has an 11-fold higher affinity for the *gadd*45 oligonuclotide (K_d = 0.89 ± 0.1 μM), in agreement with the previously reported value of 0.8 μM (*23*). ApoDBD, however, exhibits the same K_d for the *gadd*45 (6.0 ± 1 μM) and nonconsensus oligonucleotides. We conclude that the L3 loop is critical for site-specific DNA binding. When its structure is disrupted by metal ion removal, DNA can still interact with the remaining binding surface but only in a weak, sequence-independent manner. Zinc loss will therefore functionally inactivate p53.

Most Hot-Spot Mutants Do Not Affect the Stability of ApoDBD. According to the stability hypothesis of p53 inactivation, mutations lower the free energy of folding to the point where DBD is unstable. Our data demonstrate that apoDBD is both thermodynamically stable and kinetically accessible. Therefore, to understand how mutations shift the balance of p53 conformational states, it is necessary to generate a complete thermodynamic model that includes parameters for the zinc-free form.

Urea unfolds apoDBD in a reversible and apparent two-state manner, as evidenced by the following observations. First, unfolding monitored by tryptophan fluorescence and CD (10 °C) reveals isosbestic points at 318 and 231 nm, respectively (not shown). Second, normalized unfolding transitions obtained by the two methods are superimposable. Third, as a test, we diluted unfolded apoDBD (in 5 M urea) 10-fold into buffer and monitored refolding by Trp fluorescence. The spectra were identical to that of the native apoDBD control after ~10 h of refolding. These control experiments validate the use of the linear extrapolation equation (*25*) to obtain thermodynamic parameters.

We next compare stability parameters of apoDBD with those of DBD. They can be directly compared because DBD, like apoDBD, unfolds by a reversible, two-state mechanism without measurable loss of bound Zn^{2+} at 10 °C (*10*). This result seems paradoxical, since Figure 2 shows that the metal ion can be rapidly lost from native DBD. The paradox is resolved by recognizing that the rate of Zn^{2+} dissociation is highly temperature dependent. At 10 °C, the dissociation half-time is much slower than the duration of the experiment, even for unfolded DBD. Figure 6A presents unfolding curves for hot-spot DBD variants, and Table 1 summarizes the resulting stability parameters. Most mutations significantly destabilize DBD, as witnessed by the spread in the transition midpoints (C_m). These results agree well with those reported earlier (*10*, *12*) with the exception of R248Q. This mutant is more stable in our conditions, probably because of the different pH and buffers used in the two studies.

The most dramatic difference observed for apoDBD is that most mutations do not appreciably affect its stability. Wild-type and mutant C_m values generally cluster together (Figure 6B, Table 1). A particularly striking finding is that the R175H alteration lowers ΔG of the zinc-bound protein by 50%, making it one of the most debilitating mutations identified to date. However, this mutation does not significantly destabilize apoDBD. Zinc loss actually appears to stabilize R175H; however, this effect is probably due to an artificially low cooperativity parameter (m) that slightly underestimates

Table 1: Stability Parameters of DBD Variants at 10 °C

variant	ΔG (kcal·mol^{-1})	m (kcal·mol^{-1}·M^{-1})	C_m (M)	$\Delta\Delta G^a$ (kcal·mol^{-1})
wt	9.35 ± 0.086	3.30 ± 0.14	2.83 ± 0.026	not applicable
R175H	4.65 ± 0.15	2.44 ± 0.15	1.91 ± 0.063	−4.70 ± 0.17
G245S	8.40 ± 0.12	3.26 ± 0.25	2.58 ± 0.037	−0.95 ± 0.15
R248Q	10.4 ± 0.23	3.43 ± 0.26	3.04 ± 0.068	1.08 ± 0.24
R249S	7.34 ± 0.031	3.02 ± 0.18	2.43 ± 0.010	−2.01 ± 0.090
R282Q	7.23 ± 0.11	2.90 ± 0.19	2.34 ± 0.035	−2.12 ± 0.14
wt apoDBD	6.47 ± 0.14	3.21 ± 0.19	2.02 ± 0.043	not applicable
R175H apoDBD	5.87 ± 0.11	2.90 ± 0.34	2.02 ± 0.039	−0.60 ± 0.18
G245S apoDBD	5.91 ± 0.050	2.92 ± 0.13	2.02 ± 0.017	−0.56 ± 0.15
R248Q apoDBD	7.21 ± 0.046	3.32 ± 0.19	2.17 ± 0.013	0.74 ± 0.15
R249S apoDBD	6.81 ± 0.16	3.24 ± 0.21	2.10 ± 0.025	0.34 ± 0.21
R282Q apoDBD	4.42 ± 0.31	2.71 ± 0.14	1.63 ± 0.12	−2.05 ± 0.34

[a] Relative to wt, within the same Zn^{2+}-binding status.

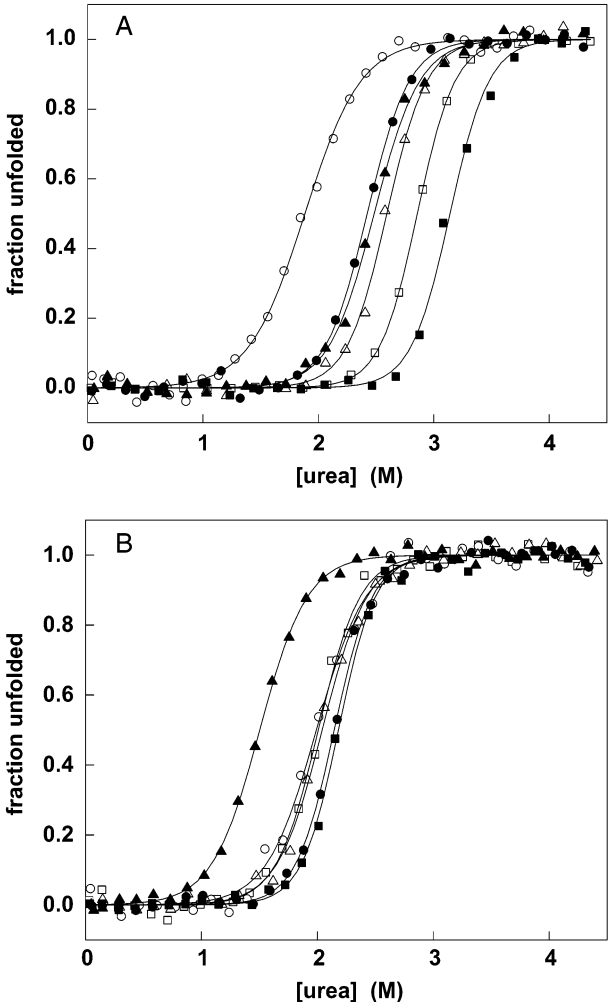

FIGURE 6: Equilibrium denaturation curves of (A) DBD and (B) apoDBD. Symbols are as follows: open squares, wt; open circles, R175H; open triangles, G245S; filled squares, R248Q; filled circles, R249S; filled triangles, R282Q. Lines are best fits of the data to the linear extrapolation equation (*25*).

the stability of R175H DBD. We found that ~15% of the R175H mutant was already in the zinc-free form immediately after purification (all other variants contained 1.0 ± 0.05 equiv of Zn^{2+}; see Materials and Methods). The small population of apoDBD likely broadens the unfolding transition of R175H DBD, resulting in a lower ΔG value when extrapolated to zero denaturant concentration.

Why do mutations affect DBD and apoDBD to such different extents? Figure 4 provides a likely explanation. All mutations except for R282Q are in regions of the protein that exhibit widespread chemical shift changes upon Zn^{2+} removal. The fact that none of these substitutions alter ΔG suggests that side chain packing interactions in these regions are altered or diminished in apoDBD. R282Q is the only mutation examined that significantly destabilizes the zinc-free form. It is located in helix H2, which HSQC spectra judge to be unperturbed. Side chain contacts apparently are similar for R282 in both the zinc-bound and zinc-free proteins.

Equilibrium denaturation studies were carried out at 10 °C because DBD is maximally stable at that temperature (*12*). We attempted to extrapolate ΔG values to 37 °C by van't Hoff analysis. Above 15 °C, however, the unfolding transition for wt apoDBD deviates from two-state behavior. The m value is 40% lower at 22 °C than its maximum value at 4 °C (3.5 kcal·mol^{-1}·M^{-1}). This trend suggests that a partially unfolded intermediate is populated at higher temperatures and at intermediate urea concentrations. In fact, above 22 °C, visible aggregation occurs at urea concentrations near the unfolding midpoint but not at higher or lower concentrations (data not shown).

Two important conclusions from the thermodynamic and structural analyses are as follows: (i) a subset of hot-spot mutations destabilizes DBD but not apoDBD, thereby increasing the population of the latter at the expense of the former; (ii) members of this class can be predicted from Figure 4. R175H is an extreme example. It is probable that R175H exists in the cell primarily in the folded zinc-free state, given its high stability and the rapid rate of Zn^{2+} loss (Figure 2). We consider the functional and physiological implications of these findings below.

ApoDBD Nucleates Aggregation of DBD. It is now widely recognized that many proteins can spontaneously assemble into insoluble fibers both in vitro and in vivo (*28*). This process is thought to be triggered by the conversion of the soluble protein to an alternate, aggregation-prone conformation. These misfolded molecules can then associate to form a nucleus from which the fiber grows. Fersht and colleagues have previously noted that some destabilizing mutations enhance the inherent tendency of wt DBD to aggregate at elevated temperatures or at intermediate urea concentrations (*10*, *12*). We find that Zn^{2+} removal has a similar effect. Therefore, we next consider the possibility that a key initial

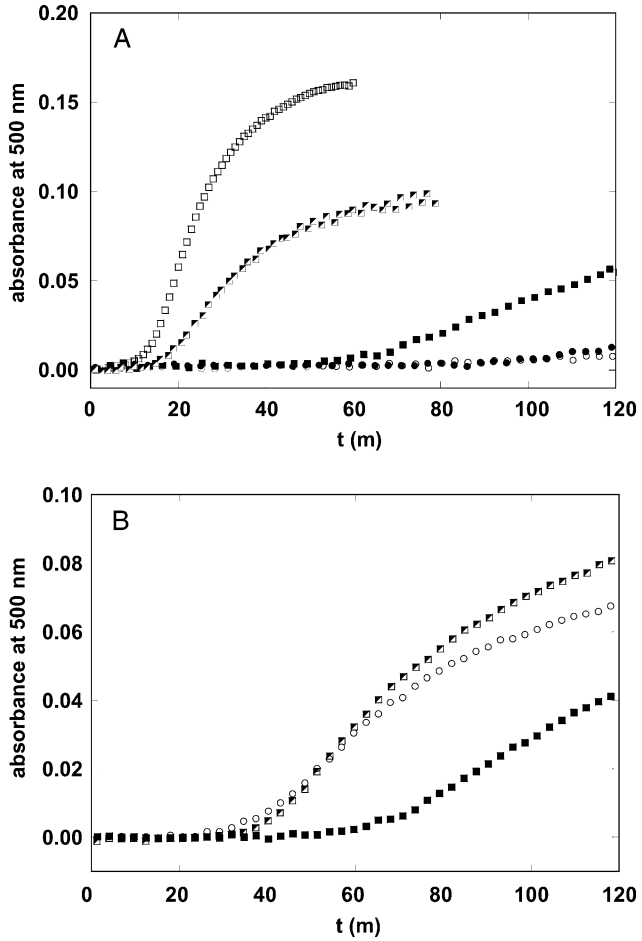

FIGURE 7: ApoDBD induces aggregation of DBD at 37 °C. Symbols are as follows: (A) filled squares, wt DBD (3.5 μM); open squares, wt apoDBD (3.5 μM); closed circles, wt DBD (2.62 μM); open circles, wt apoDBD (0.88 μM); half-filled squares, mixture of wt apoDBD (0.88 μM) and wt DBD (2.62 μM); (B) closed squares, wt DBD (3.5 μM); half-filled squares, mixture of wt apoDBD (0.88 μM) and wt DBD (2.62 μM); circles, mixture of R175H apoDBD (0.88 μM) and wt DBD (2.62 μM).

step in p53 aggregation is loss of Zn^{2+} and that the zinc-free species can serve as a nucleus.

Figure 7A shows that both DBD and apoDBD precipitate at 37 °C in the absence of urea, as monitored by 500 nm light scatter. The appearance of turbidity follows classic nucleation-growth kinetics. It exhibits a pronounced lag period that decreases with increasing protein concentration followed by an exponential growth phase. At equivalent concentration, the lag phase is much shorter for the zinc-free species. To test whether apoDBD can nucleate aggregation of DBD, we mixed 0.88 μM of the former with 2.62 μM of the latter. The 1:3 ratio was chosen to mimic the condition where one p53 monomer has lost its Zn^{2+} (full-length p53 exists as a tetramer in the cell). If apoDBD and DBD do not interact, the observed curve will simply be the sum of the two independent aggregation events. If they do interact, the increase in light scatter should be similar to the 3.5 μM DBD control except with a reduced lag time.

The results clearly point to the second scenario (Figure 7A). Neither the 0.88 μM apoDBD nor the 2.62 μM DBD samples aggregate significantly over the course of the experiment. When they are mixed, turbidity appears much faster than the 3.5 μM DBD control and nearly as fast as the 3.5 μM apoDBD control. As a further test, we repeated the experiment using R175H apoDBD and wt DBD in the same 1:3 ratio. The R175H mutation does not appear to affect the structure or stability of the zinc-free form (Table 1); it only enhances the rate of Zn^{2+} loss (Figure 2). Wild-type and R175H apoDBDs are thus expected to accelerate precipitation to similar extents. Figure 7B shows that this is indeed the case.

These findings strongly suggest that apoDBD can effectively convert soluble DBD to the aggregated form. A critical test of this hypothesis is to monitor aggregation at a urea concentration where DBD is folded and apoDBD is unfolded. The model predicts that aggregation will be inhibited under these conditions, since the putative nucleating species is unstable. Aggregation of wt DBD and wt apoDBD is largely abolished by 1.2 M urea (Figure 8A) and 0.8 M urea (not shown), respectively. These values presumably reflect the minimum concentrations required to destabilize each species to the point where nucleation cannot occur. The difference in [urea] is consistent with the higher thermodynamic stability of the zinc-bound state (Table 1). To further decrease the urea concentration needed to denature apoDBD, we used the R282Q variant. Precipitation of R282Q apoDBD is prevented by 0.4 M urea, again consistent with its lower stability relative to wt (Figure 8B).

Aggregation kinetics of a 1:3 mixture of R282Q apoDBD: wt DBD are presented in Figure 8C; 0.5 M urea eliminates the aggregation-enhancing effect of R282Q apoDBD. The 1:3 mixture exhibits nearly identical aggregation kinetics as the wt only control; it is as if R282Q is not present at all. These results prove that substoichiometric amounts of apoDBD can efficiently nucleate aggregation of DBD at 37 °C.

A Model for Zinc Loss-Mediated p53 Inactivation. We have shown that the rate of Zn^{2+} loss is accelerated by elevated temperatures and by the presence of the tumorigenic R175H mutation (Figure 2). Moreover, the majority of mutations examined decrease the stability of the zinc-bound state but not that of the zinc-free form (Table 1). An inevitable consequence is that the population of apoDBD will be elevated in cells harboring these mutant alleles. Zinc release by itself inactivates p53, as witnessed by the elimination of site-specific DNA binding activity (Figure 5). The light scatter experiments (Figures 7 and 8), however, reveal that the deleterious effect of zinc loss is amplified by an aggregation mechanism.

According to this model, metal ion release leads to a conformational change centered around the L2 and L3 loops (Figure 4). This new conformation is highly aggregation prone. It readily precipitates on its own, but more importantly, it facilitates conversion of active, soluble DBD to an insoluble aggregate via a nucleation-growth process similar to that of amyloid fiber formation.

Perhaps the most physiologically significant aspect of the model is that it provides a molecular explanation for the dominant-negative phenotype exhibited by many p53 mutations in vitro (*29*−*31*) and in vivo (*32*, *33*). This effect has been previously attributed to the cooperative nature of DNA binding which predicts that a mutant subunit that fails to bind DNA will lower the overall affinity of the tetramer by a disproportionate amount (*22*). Our data, however, suggest that p53 aggregation may be a contributing factor. We

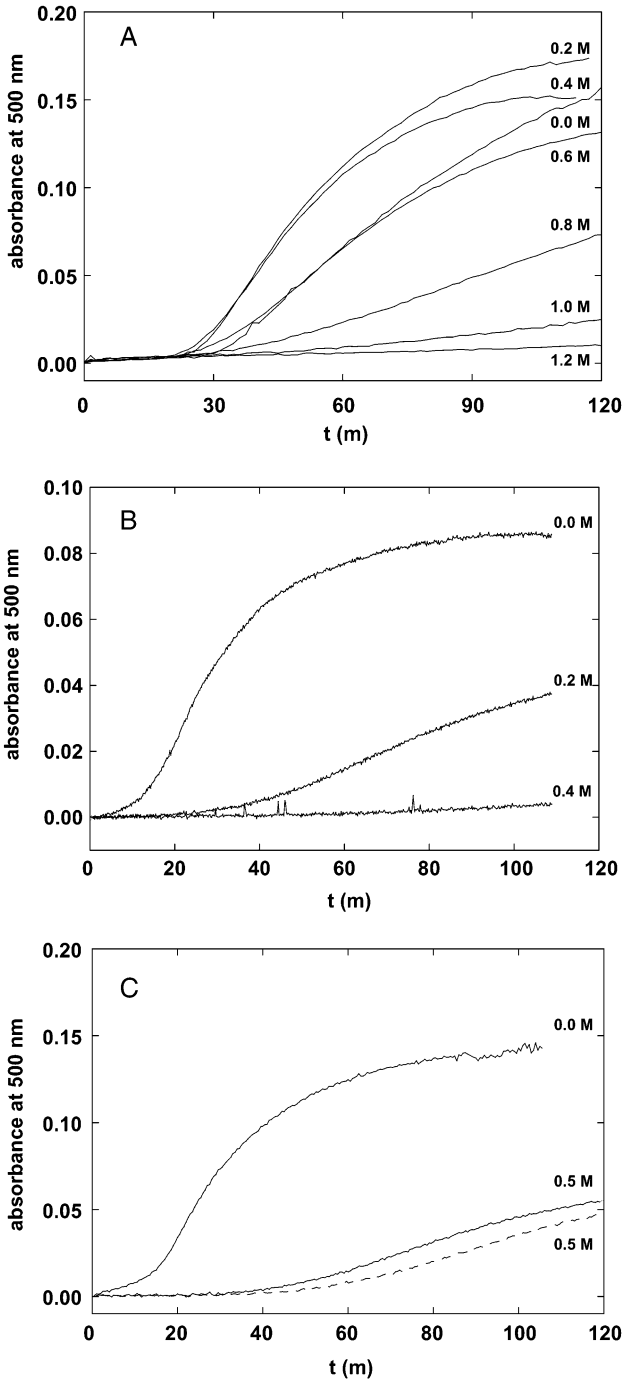

FIGURE 8: Destabilizing apoDBD by urea inhibits aggregation at 37 °C. Urea concentrations are indicated in each panel. DBD variants shown are as follows: (A) wt DBD (3.5 μM), (B) R282Q apoDBD (2.3 μM), and (C) mixture of R282Q apoDBD (0.88 μM) and wt DBD (2.62 μM) (solid lines); wt DBD (2.62 μM) (dashed line).

suggest that the process begins when a mutant monomer of a wt/mutant heterotetramer loses its zinc ion. It then associates with the remaining zinc-bound subunits, thereby inactivating the entire tetramer. Moreover, it is easily conceivable that the converted, inactive tetramer can further recruit functional tetramers to form larger aggregates similar to those seen in our light scattering studies.

A critical question is to what extent our proposed aggregation mechanism modulates p53 activity in vivo. If p53 forms large inclusion bodies in the cell, then they should be detectable by immunohistological techniques. Human neuroblastoma cells that overexpress wt p53 accumulate the protein in the form of discrete, punctuate structures in the cytoplasm with no detectable staining in the nucleus (*34*). Ultracentrifugation sedimentation analysis revealed these structures to be large molecular weight aggregates. Chinese hamster MTX M neuroblastoma cells, also overexpressing wt p53, show similar puncate p53 staining patterns in the cytoplasm only (*35*). These high molecular weight particles were resistant to denaturation by sodium dodecyl sulfate and dithiothreitol treatment, indicating that they are stable aggregates. Hot-spot mutations have been found to increase p53 accumulation in both the cytoplasm and nucleus, suggesting that mutation can induce aggregation in both compartments. Rat glioma cells expressing a temperature-sensitive V135 mutant exhibit nuclear staining with dot-like inclusions (*36*). Upon heating at 42 °C, a human pancreatic cell line harboring a mutation at R273 displays dense p53 bodies that accumulate just outside the nucleus (*37*). A systematic study of 75 colorectal cancer cell lines found that the most aggressive tumors exhibited increased p53 staining in both the nucleus and the cytoplasm (*38*). These cell lines contained mutations at R175. Finally, cell fusion experiments support our mechanism of dominant-negative behavior. When the MTX M cells (which sequester p53 in large cytoplasmic bodies) were fused with Chinese hamster B7 neuroblastoma cells (which show normal nuclear p53 localization), p53 was found to accumulate exclusively in the cytoplasm (*35*). Cytoplasmic localization is thus a dominant phenotype. The authors suggested that formation of stable p53 multimers was responsible for defective nuclear localization.

The partitioning between active (soluble) and inactive (insoluble) p53 will in large part depend on the relative concentrations of p53 and free Zn^{2+} in the cell. Once the metal ion is lost, there is a kinetic competition between rebinding and aggregation. At high $[Zn^{2+}]_{free}$, rebinding will be rapid with respect to protein−protein association and p53 will remain soluble and functional. If $[Zn^{2+}]_{free}$ is low, the aggregating nucleus is formed before Zn^{2+} can rebind. The concentration of free Zn^{2+} in mammalian cells is not precisely known. It is, however, tightly regulated by metal binding proteins such as metallothionein and has been estimated to be 10^{-6}−10^{-12} M, depending on the cell type and assay employed (*39*). Overexpression of metallothionein has been found to be an early marker of colorectal carcinoma (*40*). The scarcity of free Zn^{2+} and the preponderance of Zn^{2+}-dependent transcription factors have led to the speculation that gene expression may be partially regulated by Zn^{2+} bioavailability (*41*).

Other factors may influence this kinetic competition as well. The effective DBD concentration will be higher than expected if the DBD monomers are held close to one another by the topology of the tetramer. The structure of the tetramer has not been solved; however, a model based on the crystal structure of monomeric DBD suggests that the DBD subunits are close enough to interact with each other within the tetramer (*7*). Finally, we note that, with ten cysteine and nine histidine residues in DBD, there is a realistic chance that Zn^{2+} may misligate once it has been released. Until now, most small molecule-based approaches for treating p53-related cancers have been directed at stabilizing mutant DBD. Our results point to an alternate strategy of preventing Zn^{2+}

loss or, failing that, of inhibiting protein aggregation long enough to allow Zn^{2+} to rebind.

ACKNOWLEDGMENT

We thank Drs. Michael Kay, Richard Cross, Farzan Rastinejad, Patricia Kane, and Jeung-Hoi Ha for critical review of the manuscript and Dr. Jeung-Hoi Ha and Tracy Radley for constructing DBD mutants.

REFERENCES

1. El-Deiry, W. S., et al. (1993) WAF1, a potential mediator of p53 tumor supression, *Cell 75*, 817−825.
2. Kastan, M. B., et al. (1992) A mammalian cell cycle checkpoint pathway utilizing p53 and GADD45 is defective in ataxia-telagiectasia, *Cell 71*, 587−597.
3. Wu, X., et al. (1993) The p53-mdm-2 autoregulatory feedback loop, *Genes Dev. 7*, 1126−1132.
4. Buckbinder, L., et al. (1995) Induction of the growth inhibitor IGF-binding protein 3 by p53, *Nature 377*, 646−649.
5. Miyashita, T., and Reed, J. C. (1995) Tumor supressor p53 is a direct transcriptional activator of the human bax gene, *Cell 80*, 293−299.
6. Bunz, F., et al. (1998) Requirement for p53 and p21 to sustain G2 arrest after DNA damage, *Science 282*, 1497−1501.
7. Cho, Y., et al. (1994) Crystal structure of a p53 tumor suppressor-DNA complex: Understanding tumorigenic mutations, *Science 265*, 346−355.
8. Kern, S. E., et al. (1992) Oncogenic forms of p53 inhibit p53-regulated gene expression, *Science 256*, 827−830.
9. Unger, T., et al. (1992) p53: a transdominant regulator of transcription whose function is ablated by mutations occurring in human cancer, *EMBO J. 11*, 1383−1390.
10. Bullock, A. N., et al. (1997) Thermodynamic stability of wild-type and mutant p53 core domain, *Proc. Natl. Acad. Sci. U.S.A. 94*, 14338−14342.
11. Wong, K.-B., et al. (1999) Hot-spot mutants of p53 core domain evince characteristic local structural changes, *Proc. Natl. Acad. Sci. U.S.A. 96*, 8438−8442.
12. Bullock, A. N., Henckel, J., and Fersht, A. R. (2000) Quantitative analysis of residual folding and DNA binding in mutant p53 core domain: definition of mutant states for rescue in cancer therapy, *Oncogene 19*, 1245−1256.
13. Meplan, C., Richard, M.-J., and Hainaut, P. (2000) Redox signaling and transition metals in the control of the p53 pathway, *Biochem. Pharmacol. 59*, 25−33.
14. Pavletich, N. P., Chambers, K. A., and Pabo, C. O. (1993) The DNA-binding domain of p53 contains the four conserved regions and the major mutation hot spots, *Genes Dev. 7*, 2556−2564.
15. Hainaut, P., Butcher, S., and Milner, J. (1995) Temperature sensitivity for conformation is an intrinsic property of wild-type p53, *Br. J. Cancer 71*, 227−231.
16. Rainwater, R., et al. (1995) Role of cysteine residues in regulation of p53 function, *Mol. Cell. Biol. 15*, 3892−3903.
17. Meplan, C., Richard, M.-J., and Hainaut, P. (2000) Metallogregulation of the tumor supressor protein p53: zinc mediates the renaturation of p53 after exposure to metal chelators in vitro and in intact cells, *Oncogene 19*, 5227−5236.
18. Verhaegh, G. W., et al. (1998) Modulation of p53 protein conformation and DNA-binding activity by intracellular chelation of zinc, *Mol. Carcinog. 21*, 205−214.
19. Maniatis, T., Fritsch, E. F., and Sambrook, J. (1986) *Molecular Cloning: A Laboratory Manual*, Cold Spring Harbor Laboratory, Cold Spring Harbor, NY.
20. Edelhoch, H. (1967) Spectroscopic determination of tryptophan and tyrosine in proteins, *Biochemistry 6*, 1948−1954.
21. Hunt, J. B., Neece, S. H., and Ginsburg, A. (1985) The use of 4-(2-pyridylazo)resorcinol in studies of zinc release from *Escherichia coli* aspartate transcarbamoylase, *Anal. Biochem. 146*, 150−157.
22. Nicholls, C. D., et al. (2000) Biogenesis of p53 involves cotranslational dimerization of monomers and posttranslational dimerization of dimers, *J. Biol. Chem. 27*, 12937−12945.
23. Friedler, A., et al. (2002) A peptide that binds and stabilizes p53 core domain: Chaperone strategy for rescue of oncogenic mutants, *Proc. Natl. Acad. Sci. U.S.A. 99*, 937−942.
24. Pace, C. N., and Scholtz, J. M. (1997) in *Protein structure: a practical approach* (Creighton, T. E., Ed.) 2nd ed., pp 299−320, Oxford University Press, New York.
25. Santoro, M. M., and Bolen, D. W. (1988) Unfolding free energy changes determined by the linear extrapolation method. 1. Unfolding of phenylmethanesulfonyl alpha chymotrypsin using different denaturants, *Biochemistry 27*, 8063−8068.
26. Fritz, G., Heizmann, C. W., and Kroneck, P. M. H. (1998) Probing the structure of the human Ca^{2+}- and Zn^{2+}-binding protein S100A3: spectroscopic investigations of its transition metal ion complexes, and three-dimensional structural model, *Biochim. Biophys. Acta 1448*, 264−276.
27. DiTusa, C. A., et al. (2001) Thermodynamics of metal ion binding. 2. Metal ion binding by carbonic anhydrase variants, *Biochemistry 40*, 5345−5351.
28. Dobson, C. M. (1999) Protein misfolding, evolution, and disease, *Trends Biochem. Sci. 24*, 329−332.
29. Milner, J., and Medcalf, E. A. (1991) Cotranslation of activated mutant p53 with wild-type drives the wild-type p53 protein into the mutant conformation, *Cell 65*, 765−774.
30. Chene, P., Mittl, P., and Grutter, M. (1997) In vitro structure-function analysis of the beta-strand 326−333 of human p53, *J. Mol. Biol. 273*, 873−881.
31. Chene, P. (1998) In Vitro analysis of the dominant negative effect of p53 mutants, *J. Mol. Biol. 281*, 205−209.
32. Aurelio, O. N., et al. (2000) p53 mutants have selective dominant-negative effects on apoptosis but not growth arrest in human cancer cell lines, *Mol. Cell. Biol. 20*, 770−778.
33. Park, D. J., et al. (1994) Transactivational and DNA binding abilities of endogenous p53 in p53 mutant cell lines, *Oncogene 9*, 1899−1906.
34. Moll, U. M., et al. (1996) Cytoplasmic sequestration of wild-type p53 protein impairs the G_1 checkpoint after DNA damage, *Mol. Cell. Biol. 16*, 1126−1137.
35. Ottaggio, L., et al. (2000) Defective nuclear localization of p53 protein in a Chinese hamster cell line is associated with the formation of stable cytoplasmic protein multimers in cells with gene amplification, *Carcinogenesis 21*, 1631−1638.
36. Klotzsche, O., et al. (1998) Cytoplasmic retention of mutant tsp53 is dependent on an intermediate filament protein (Vimentin) scaffold, *Oncogene 16*, 3423−3434.
37. Mogaki, M., et al. (1993) Comparison of p53 protein expression and cellular localization in human and hamster pancreatic cell lines, *Carcinogenesis 14*, 2589−2594.
38. Jansson, A., Gentile, M., and Sun, X.-F. (2001) p53 Mutations are present in colorectal cancer with cytoplasmic p53 accumulation, *Int. J. Cancer 92*, 338−341.
39. Sensi, S. L., et al. (1997) Measurement of Intracellular Free Zinc in Living Cortical Neurons: Routes of Entry, *J. Neurosci. 17*, 9554−9564.
40. Bruewer, M., et al. (2002) Metallothionein: early marker in the carcinogenesis of ulcerative colitis-associated colorectal carcinoma, *World J. Surg. 26*, 726−731.
41. DeMoor, J. M., and Koropatnick, D. J. (2000) Metals and signaling in mammalian cells, *Cell. Mol. Biol. 46*, 367−381.

BI026635N